Iridium clusters for catalytic partial oxidation of methane—an *in situ* transmission and fluorescence XAFS study

J.-D. Grunwaldt [a,*], P. Kappen [b], L. Basini [c], and B.S. Clausen [a]

[a] *Haldor Topsøe A/S, Nymøllevej 55, DK-2800 Lyngby, Denmark*
[b] *Hamburger Synchrotronstrahlungslabor HASYLAB at Deutsches Elektronen-Synchrotron DESY, Notkestraße 85, D-22603 Hamburg, Germany*
[c] *Snamprogetti S.p.A., Via Maritano 26, I-20097 S. Donato Milanese (MI), Italy*

Received 21 August 2001; accepted 8 September 2001

In situ transmission and fluorescence EXAFS combined with on-line gas analysis have provided new insight in the structural changes and the catalytic properties of Ir clusters during the catalytic partial oxidation (CPO) of methane. A novel *in situ* fluorescence XAFS setup with a multi element silicon drift detector allows time-resolved *in situ* studies on catalysts with small noble metal concentrations. Significant structural differences were found between a 0.5 wt% Ir/Al_2O_3 and a 2.5 wt% Ir/Al_2O_3 catalyst upon treatment in He and H_2. After He treatment metallic clusters form on high loading Ir catalysts but not when the loading is small. Upon H_2 treatment metallic Ir clusters are detected in both catalysts, but the particle size is smaller when a low loading is used. The smaller clusters appear to be more sensitive to oxidation. The CPO reaction is found to ignite at 320 °C, nearly independent of the residence time and the Ir cluster size. The structure of the clusters changes significantly at the ignition point. Below the ignition point they are partly (2.5 wt% Ir) or nearly fully (0.5 wt% Ir) oxidized and above the ignition temperature they are abruptly reduced. The catalytic and structural changes are reversible.

KEY WORDS: CPO; iridium; clusters; EXAFS; fluorescence; *in situ*

1. Introduction

Small noble metal based clusters have interesting catalytic properties for a number of different chemical reactions. Therefore, their physicochemical properties are of considerable interest. In particular the possibility to define a link between the reactivity and the structure of reacting clusters will improve the conceptual design of catalysts devoted to a specific reaction.

One of the potentially interesting areas for small noble metal based clusters such as Pt-, Pd-, Ru-, Rh-, and Ir-containing clusters [1–8] is the catalytic partial oxidation of methane to synthesis gas. Small metallic Ir, Rh and Ru particles can be prepared by fixation of their corresponding tetrametallic carbonyl clusters on an oxide surface [4,7,9–16] and subsequent decomposition and reduction. Using this preparation procedure, we focused in this study on the Ir/Al_2O_3 system and studied the structure of the Ir clusters during preparation, activation and under CPO reaction conditions.

In order to elucidate the structure of the noble metal clusters in the CPO reaction, *in situ* studies are vital because the active species are usually only formed during the catalytic reaction. Due to the high dispersion of the noble metal in the catalysts, X-ray absorption fine structure is an ideal technique to identify the structure of such clusters under reaction conditions [17–25]. Recently, we reported studies of the catalytic partial oxidation of methane on Rh/Al_2O_3 catalysts [26]. The Rh clusters changed their structure significantly upon ignition of the CPO reaction (reduction and disruption of larger clusters). The comparison of XAFS results on high loading Rh/Al_2O_3 catalysts with results from diffuse reflectance infrared Fourier transform spectroscopy (DRIFTS) studies on catalysts with lower loading indicated different reactivity of the clusters [26]. While oxidized Rh clusters are reduced at high temperatures in a CH_4 atmosphere (>200 °C) when the Rh loading is high they are already reduced at room temperature when the Rh loading is low.

Typically, the metal loading of CPO catalysts is relatively low and time-resolved transmission XAFS experiments are not feasible. In this respect, fluorescence XAFS is a powerful technique [27–31]. It has recently been shown that by the use of a silicon drift detector (SDD) sufficient count rates can be obtained so that *in situ* studies on catalysts with a relatively low loading of the element of interest (a few 100 ppm) are possible [29,30]. In addition, when an *in situ* cell is combined with on-line mass analysis (as applied in transmission XAFS experiments previously [22,24,32,33]) simultaneous catalytic measurements become possible.

Here we present results obtained by XAFS in the fluorescence mode on low loading Ir/Al_2O_3 catalysts (*ca.* 0.5 wt% Ir) under reaction conditions and compare them with transmission XAFS results obtained on higher loading Ir/Al_2O_3 catalysts. For this purpose, Ir catalysts prepared by the deposition of $Ir_4(CO)_{12}$ on alumina were used in a sequence of reactions encompassing the treatment in He, H_2, and the reaction mixture CH_4/O_2. This sequence is similar to previous DRIFTS and XAFS studies on Rh/Al_2O_3 catalysts [4,26]. A capillary tube served as reaction cell with on-line gas

* Present address: ETH Zürich, Department of Technical Chemistry, Universitätsstr. 6, CH-8092 Zürich, Switzerland.

1011-372X/02/0300-0013/0

analysis and as *in situ* cell for XAFS in the fluorescence and transmission detection mode. In this way, on-line catalytic data and structural data could be obtained simultaneously on the same sample. The results are discussed with respect to previous results on Rh/Al_2O_3 catalysts by XAFS [26] and DRIFTS results on similar Ir/Al_2O_3 catalysts [4,7].

2. Experimental

The synthesis of the Ir/Al_2O_3 samples was performed by adding slowly an anhydrous THF solution of $Ir_4(CO)_{12}$ under CO atmosphere into a slurry of α-Al_2O_3 (Aldrich, 99.999 wt%). Further details are described in [4]. The loading of Ir in the two samples in the present study amounted to 0.5 and 2.5 wt% Ir on Al_2O_3, respectively.

The 2.5 wt% Ir/Al_2O_3 sample (sample A) was investigated with transmission XAFS while the 0.5 wt% Ir/Al_2O_3 sample (sample B) was subjected to fluorescence XAFS studies. In both cases, three subsequent experiments with decomposition of the Ir-carbonyl precursor and activation of the catalysts were performed in He, H_2, and CH_4/O_2, as shown in the following scheme:

$$\mathrm{A} \xrightarrow[25-500\,^\circ\mathrm{C}]{\mathrm{He}} \mathrm{B} \quad \text{(step I)} \tag{1}$$

$$\mathrm{B} \xrightarrow[25-500\,^\circ\mathrm{C}]{\mathrm{H_2}} \mathrm{C} \quad \text{(step II)} \tag{2}$$

$$\mathrm{C} \xrightarrow[25-600\,^\circ\mathrm{C}]{\mathrm{CH_4 + O_2}} \mathrm{D} \quad \text{(step III)} \tag{3}$$

For this purpose gasses of pure He, 2% H_2/N_2, and 6% CH_4/3% O_2/Ar were used. Typically, a heating rate of 5 °C/min was applied to reach the corresponding reaction temperature. Afterwards, the samples were rapidly cooled from the reaction temperature to room temperature. Typically, a flow of 5 ml/min was used but during reaction (step III) two flow rates were applied; 1 and 17 ml/min in the case of transmission XAFS, corresponding to residence times around 0.54 and 0.03 s. During FLEXAFS experiments the flow was varied between 1 and 20 ml/min (residence times 1.0 and 0.05 s).

The *in situ* XAFS experiments in the transmission and the fluorescence mode combined with on-line mass analysis were performed at the Hamburg Synchrotron Laboratory (HASYLAB) at bending magnet and wiggler beamlines X1 and BW1, respectively. A quartz capillary tube served both as reaction cell and *in situ* XAFS cell. The capillary cell was heated by a controlled stream of hot nitrogen and temperature homogeneity was ensured by enclosing the *in situ* cell in an X-ray transparent heat shield (25 μm Capton foil). The outlet gas was analyzed using a mass spectrometer (Balzers Thermostar). More details on the setup are described in [22,29,30,32,33].

For the XAFS experiments in the transmission mode, the samples (*ca*. 10 mg, sieve fraction 75–125 μm) were loaded in a capillary cell with diameter $\varnothing = 0.5$ mm (wall thickness $d = 0.01$ mm). EXAFS spectra were recorded under stationary reaction conditions around the Ir L_3 edge between 11000 and 12600 eV. A Ta-foil (Ta L_2 edge, 11132.0 eV) was used as energy reference. QEXAFS data were collected under dynamic conditions in the 11000–11500 region (5 min/scan). The X-rays were monochromatized using a Si(111) double crystal monochromator and the content of higher harmonics was diminished by detuning the two crystals from the parallel position. Fourier transformation was applied on the k^1-, k^2-, and k^3-weighted $\chi(k)$ function in the interval $k = 2.5$–15.0 Å. The dominating peak in the Fourier transform was filtered and then backtransformed into k-space. Since Ir and Pt are adjoining neighbors in the periodic table (on the transferability, *cf.* [34,35]), the backscattering amplitudes and phase shifts of the Ir–Ir and Ir–O contributions were taken from the Pt-references, Pt foil and $H_2Pt(OH)_6$, respectively.

For XAFS experiments in the fluorescence mode, a quartz capillary with a slightly larger diameter ($\varnothing = 0.7$ mm, $d = 0.01$ mm, sieve fraction 75–125 μm, *ca*. 20 mg) was used. The fluorescence X-rays were detected with a seven element silicon drift detector, which was operated at room temperature. The SDD was placed in a 90° angle to the beam and a 60° angle to the *in situ* cell. Further details on the *in situ* fluorescence setup are given in, *e.g.* [29,30]. The fluorescence EXAFS spectra were recorded in the energy range 11050–12000 eV (acquisition time 30–60 min). XANES scans during dynamic changes were performed in the energy range 11190–11310 eV (7 min/scan).

The seven individually recorded fluorescence XAFS spectra were corrected for the dead time of the detection system and added up using weighting factors determined by the statistical quality of each of the scans. The resulting fluorescence XAFS spectrum was then normalized to an edge jump of 1. Fourier transformation was applied on the k^1-weighted $\chi(k)$ function in the interval $k = 2.5$–12.0 Å. The dominating peak in the Fourier transform was filtered and then backtransformed into k-space.

3. Results and discussion

3.1. Decomposition of $Ir_4(CO)_{12}/Al_2O_3$ in He and H_2 (steps I and II)

The as-prepared catalyst samples A (2.5 wt% Ir/Al_2O_3) and B (0.5 wt% Ir/Al_2O_3) exhibited DRIFTS spectra with absorption bands for the CO stretching frequencies at 2110, 2035, 2010, and 2001 cm^{-1}. The multiplicity of the IR signals are consistent with spectra produced by small hydridoclusters such as $HIr_4(CO)_{11}^-$ [4,7,13,36], which could be formed through the solid–liquid reaction between the alumina support and the $Ir_4(CO)_{12}$ clusters as proposed in other studies [10,11]. In EXAFS, a strong whiteline was observed for both samples (*cf.* selected energy region in figure 1). A stronger whiteline of carbonyl clusters compared to Ir metal is typical and has been reported previously (*e.g.*, Zhao

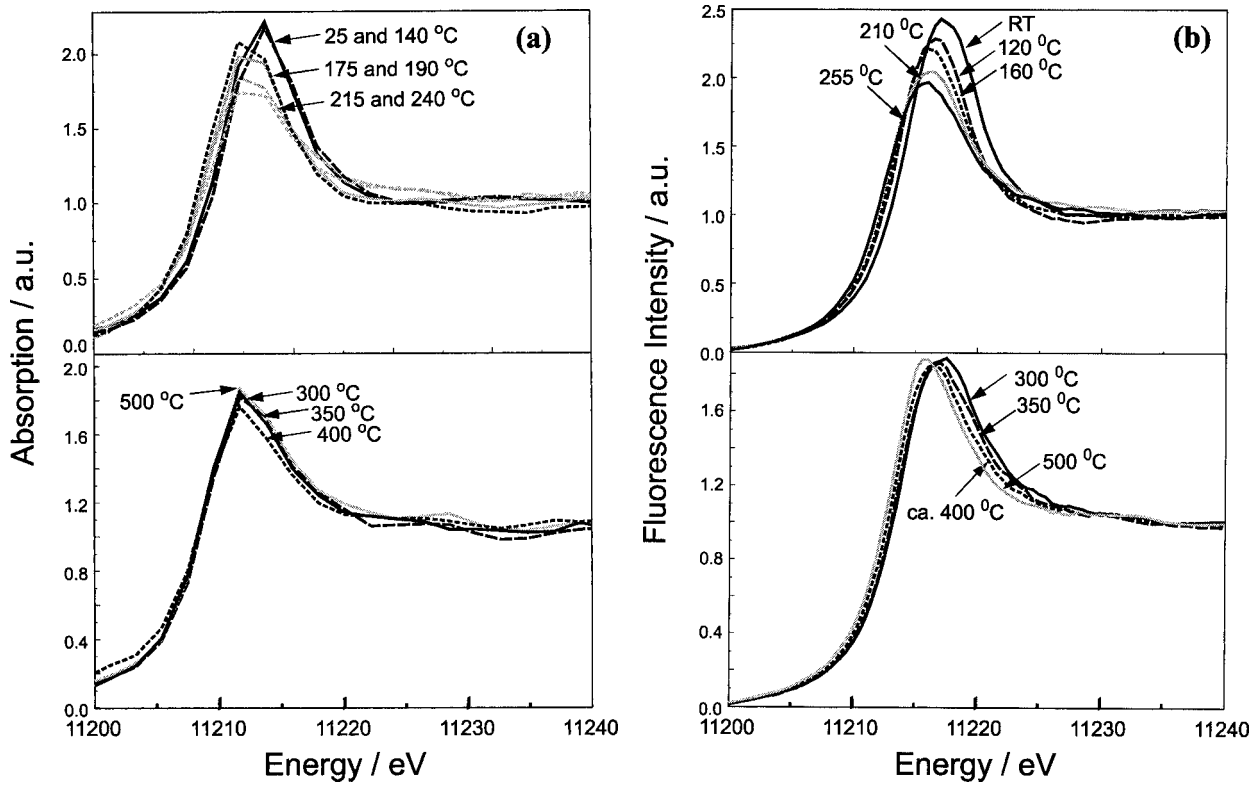

Figure 1. Selected *in situ* XANES data at the Ir L_3 edge during heating in He to 500 °C: (a) on 2.5 wt% Ir/Al_2O_3 in the transmission mode and (b) on 0.5 wt% Ir/Al_2O_3 with fluorescence detection.

and Gates [14]). The fit of the Ir–Ir shell was quite poor when considering only Ir backscatters in the first shell (table 1).

Figure 1 gives an overview on the XANES spectra of samples A and B during heating in He to 500 °C (step I). The near edge region can be resolved both on the 2.5 and the 0.5 wt% Ir sample. Since a continuous heating ramp of 5 °C/min was used, a spectrum was obtained *ca.* every 25 °C (transmission XANES) and 35 °C (fluorescence XANES), respectively. In both cases, the structure of the sample started to change around 160 °C. A release of CO_2 was simultaneously detected by the mass spectrometer on the 2.5 wt% Ir/Al_2O_3 sample (figure 2).

After He treatment of sample A not only the whiteline decreased in the XANES spectra (figure 1(a)), but also an increased number of EXAFS oscillations were observed after the decomposition in He at $E > 11220$ eV (*cf.* figure 7). This indicates the formation of metallic clusters after decomposition at elevated temperatures and is a typical difference between oxidized/carbonyl and metallic Ir clusters [11,14]. Also the results from fitting (table 1) support this interpretation. After He treatment there is a significantly higher contribution from Ir backscatters than for the untreated sample (table 1). The coordination number N_{Ir-Ir} is about 9 (typical quality of the fits $\chi^2 = \sum(\chi^2_{obs} - \chi^2_{calc})/\sum \chi^2_{obs} < 0.05$, unless otherwise stated). Other authors [10,11] have found, *e.g.*, for Ir on MgO, Al_2O_3 or zeolite as support and more gentle treatment (He, 300 °C), that the Ir coordination num-

Table 1
EXAFS parameters (coordination number N and Ir–Ir distance R_{Ir-Ir}) of RT spectra of sample A after the different reaction steps (fit of Ir–Ir shell, k^1-weighted functions, backscattering amplitudes and phase shifts taken from the Pt-foil as reference, backtransform between 1.2 and 3.3 Å)

Catalyst	Treatment	N_{Ir-Ir}	R_{Ir-Ir} (Å)	σ (Å)	ΔE (eV)
Ir/Al_2O_3	As received	–	–	–	–[a]
Ir/Al_2O_3	After He	8.8	2.73	0.085	2.2
Ir/Al_2O_3	After 2% H_2	10.8	2.72	0.082	1.26
Ir/Al_2O_3	After CH_4/O_2	9.7	2.73	0.072	0.31

[a] Insufficient fit of the Ir–Ir shell ($\chi^2 \gg 0.05$).

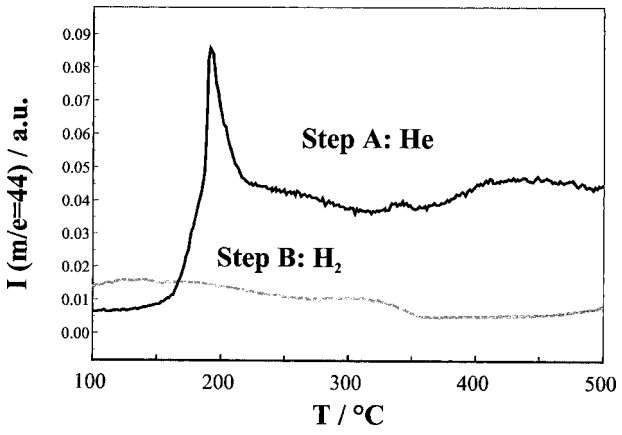

Figure 2. Trace of $m/e = 44$ (CO_2) in the mass spectrometer on sample A (2.5 wt% Ir/Al_2O_3) during treatment in He (step I) and H_2 (step II).

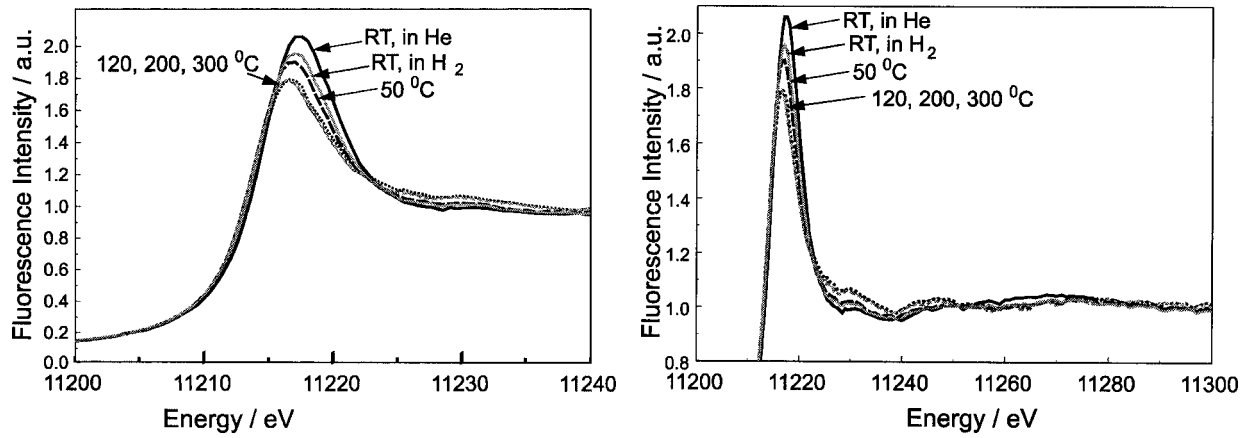

Figure 3. Selected *in situ* XANES data (recorded in the fluorescence mode) at the Ir L_3 edge during heating in H_2 on 0.5 wt% Ir/Al_2O_3.

ber stayed small ($N_{Ir-Ir} < 5$). Therefore, Ir_4 or Ir_6 clusters were assumed to be preserved. This is not observed on the alumina support used in this study. The behavior of sample A (2.5 wt% Ir/Al_2O_3) in He is very similar to a sample containing 5 wt% $Rh_4(CO)_{12}$ on alumina, described previously in [26]. In this previous study we also observed decarbonylation and the formation of metallic Rh clusters after treatment in He at 500 °C.

Sample B (0.5 wt% Ir/Al_2O_3) shows similar changes at the whiteline around 160 °C upon He treatment but there are no evident changes in the XANES region at higher temperatures. In this case, the fit of the first shell is relatively poor, when assuming only Ir–Ir coordination, which could indicate Ir–O and Ir–C contributions. Moreover, the whiteline is still high after He treatment (*cf.* figure 3). This supports results from DRIFTS, where studies on 0.25 wt% Ir/Al_2O_3 were performed and it was concluded that $Ir^I(CO)_2$ species under CO_2 release were formed [4]. Due to the lower loading, aggregation and therefore, the formation of metallic clusters appear not to be as pronounced as in sample A.

When samples A and B are reduced in H_2 (step II), significant changes in the near edge region are observed for sample B (0.5 wt% Ir/Al_2O_3, figure 3). The whiteline decreases already at room temperature and stronger EXAFS oscillations are observed at $E > 11220$ eV after reduction. No pronounced changes in the near edge region are observed for sample A in the XANES region when it is heated to 500 °C. This supports the conclusion that the extent of metallic Ir particles after He treatment is higher in the case of sample A.

The results from the fitting are given in tables 1 and 2 (k^1 weighting) and they show that the Ir–Ir shell of both the transmission and fluorescence EXAFS data can be readily extracted. Principally, the same data were obtained for k^2 and k^3 weighting of the transmission XAFS data. For fluorescence EXAFS was found to be best when using k^1 weighting. For sample A (2.5 wt% Ir/Al_2O_3), the formation of larger metallic clusters (higher coordination number of the Ir–Ir shell) compared to those formed after He treatment was observed upon reduction in H_2. In addition the formation of methane was detected by the mass spectrometer, indicating that some carbonyl clusters remained on the support after step I. The structural changes during H_2 treatment are similar to the recent results on Rh/Al_2O_3, where the Rh clusters were observed to sinter significantly upon reduction in H_2 and residual carbon and oxygen species were removed.

The investigation of sample B by fluorescence XAFS showed that the whiteline decreased significantly due to the decomposition of the $Ir^I(CO)_2$ species and that metallic iridium clusters form. Compared to sample A, the coordination number and therefore also the Ir particle size is significantly smaller (table 2). Therefore, the dispersion of Ir appears to be higher in sample B. Note that the fluorescence XAFS spectra were not corrected by the self-adsorption. The influence of self-absorption, however, is expected to be small due to the low concentration of the metal of interest. The Ir–Ir distance of 2.72 Å corresponds well to the value of 2.71 Å in bulk Ir. We have also analyzed two sequential spectra to show the reliability of the analysis and both datasets are included in table 2 (after reduction in 2% H_2/N_2). While we have used the SDD in previous studies [29–31] mainly to record XANES data, this analysis shows that this detector can also be used to obtain good quality *in situ* fluorescence EXAFS data in a relatively short time period (30–60 min).

Table 2
EXAFS parameters (coordination number N and Ir–Ir distance R_{Ir-Ir}) of RT spectra of sample B recorded in the fluorescence mode after the different reaction steps (fit of Ir–Ir shell, k^1-weighted functions, backscattering amplitudes and phase shifts taken from the Pt-foil as reference, backtransform between 1.2 and 3.3 Å)

Catalyst	Treatment	N_{Ir-Ir}	R_{Ir-Ir} (Å)	σ (Å)	ΔE (eV)
Ir/Al_2O_3	As received	–	–	–	–[a]
Ir/Al_2O_3	After He	4.5	2.70	0.08	4.65[b]
Ir/Al_2O_3	After 2% H_2	8.2	2.71	0.07	1.77
Ir/Al_2O_3	After 2% H_2	8.7	2.71	0.07	1.45
Ir/Al_2O_3	After CH_4/O_2	6.4	2.70	0.07	5.39[b]

[a] Insufficient fit of the Ir–Ir shell ($\chi^2 \gg 0.05$).
[b] Relatively poor fit ($\chi^2 > 0.05$).

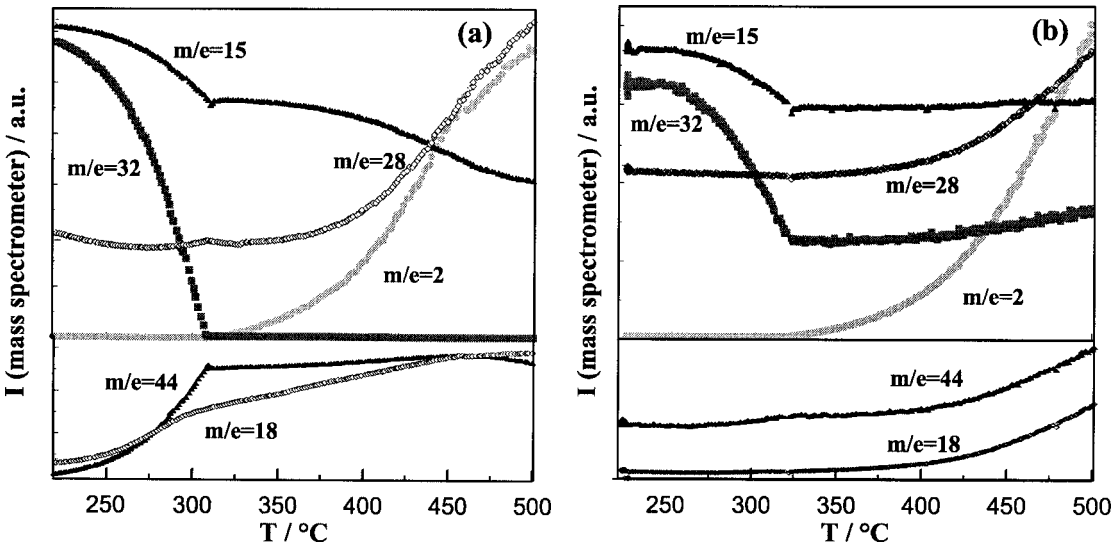

Figure 4. Traces of different MS signals in the reaction mixture CH_4/O_2 (step III, 17 ml/min) on (a) sample A (2.5 wt% Ir/Al_2O_3) and (b) sample B (0.5 wt% Ir/Al_2O_3) with signals for the educts (CH_4 $m/e = 15$; O_2 $m/e = 32$), the products (H_2 $m/e = 2$; CO $m/e = 28$), and the by-products (H_2O $m/e = 18$; CO_2 $m/e = 44$), MS data (not calibrated, different intensity) recorded simultaneously to XANES data in the transmission and fluorescence mode (figures 5 and 6, respectively).

3.2. Ir/Al_2O_3 under CPO reaction conditions (step III)

After hydrogen treatment and the formation of metallic Ir clusters on the alumina surface, samples A and B were heated in the CPO reaction mixture to 600 °C. Figure 4 depicts the traces detected in the mass spectrometer for the products H_2 ($m/e = 2$) and CO ($m/e = 28$), and the reactants methane ($m/e = 15$) and oxygen ($m/e = 32$). The CPO reaction ignited at about 320 °C, which is apparent from the MS traces. A similar behavior has been found for Rh/Al_2O_3 catalysts [26].

There is no difference in the ignition temperature between the two catalysts A and B and their behavior is similar to Rh clusters on alumina prepared by the same method. In both cases, total oxidation of methane to CO_2 and H_2O dominates below the ignition temperature (figure 4). The selectivity towards CO/H_2 improves significantly at higher temperatures, in agreement with most observations in the literature [7,8,37].

Figures 5 and 6 illustrate the structural changes around the ignition point for catalysts A (2.5% Ir/Al_2O_3) and B (0.5% Ir/Al_2O_3), respectively. The whiteline around 300 °C in the CPO reaction mixture is higher than after reduction in step II. Moreover, an increase of the whiteline is observed for both catalysts while heating the catalyst in the CPO reaction mixture to the ignition point (similar to Rh/Al_2O_3). Above the ignition temperature of 320 °C, a sudden decrease in the whiteline for catalyst A (figure 5) and catalyst B (figure 6) occurs.

Concerning catalyst A the strong EXAFS oscillations above 11220 eV, typical for metallic particles, are present in all spectra (figure 5(a)). This indicates that Ir is also at least partly present in metallic form at temperatures below the ignition point. This is supported by the fact that the whiteline is lower than typically observed for Ir_2O_3.

The structural changes of sample B during heating of the 0.5 wt% Ir/Al_2O_3 catalyst are much more pronounced than for sample A, *i.e.*, the decrease of the whiteline is significantly stronger around the ignition temperature (figure 6). Moreover, for $T > 320$ °C the number of XAFS oscillations at $E > 11220$ eV is higher than in the spectra at a temperature of 265 and 300 °C. As outlined above, the whiteline increased significantly when the gas stream was changed after step II from H_2 to CH_4/O_2 in step III and when the sample was heated to the ignition temperature. This reveals that Ir in sample B is significantly oxidized when it is heated to 320 °C in the CPO gas mixture. Additionally, it appears that the extent of metallic Ir particles is smaller just below the ignition point compared to sample A with higher Ir loading. The sensitivity of the Ir clusters towards oxygen in the 0.5 wt% Ir/Al_2O_3 sample may be higher, *e.g.*, due to smaller particle size (*cf.* discussion later in this section). The ignition point of the CPO reaction is located at about the same temperature as for the higher loaded Ir/Al_2O_3 sample (*cf.* figure 4 (a) and (b)) and also the structural changes (*cf.* figures 5 and 6) occur in the same temperature interval. Above the ignition point and at reaction temperatures ($T > 500$ °C), Ir in sample B is in a metallic state similar to sample A. DRIFTS studies have also indicated structural changes around 300 °C [7]. Above this temperature carbonyl species were detected by infrared spectroscopy on the Ir surface.

When catalysts A and B are quickly cooled (in less than 1 min) from the reaction temperature to room temperature, sample A maintains Ir in the metallic state while the Ir clusters on sample B are oxidized, as can be seen by a higher whiteline after cooling to room temperature. Therefore, the Ir–Ir shell in sample A (2.5 wt% Ir/Al_2O_3) can be well fitted (table 1) with a single Ir–Ir scattering, while the first backscatter peak in sample B has especially contributions from other atoms than Ir (table 2).

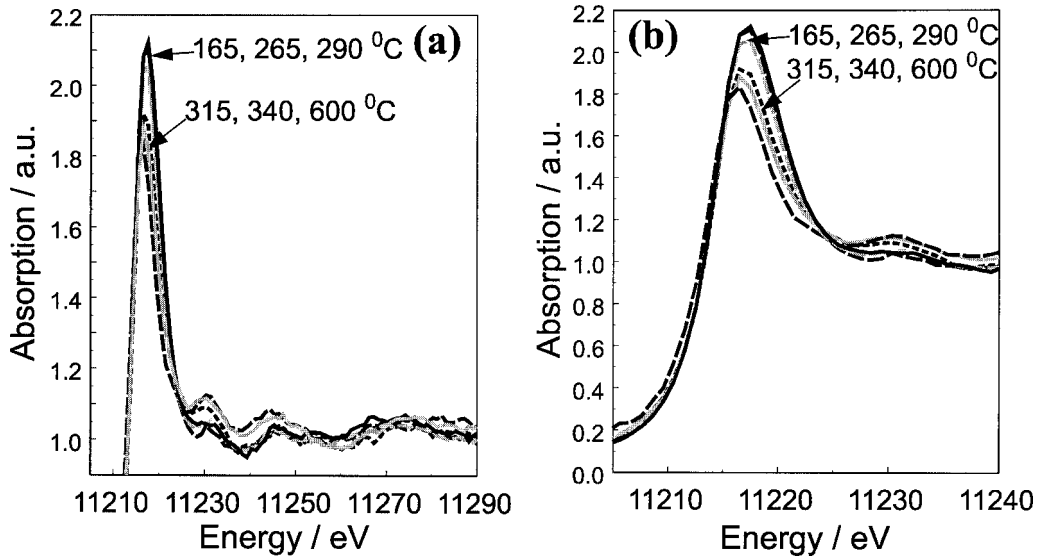

Figure 5. Selected *in situ* XANES data (transmission mode) at the Ir L_3 edge below and above the ignition temperature of the CPO reaction in the reaction mixture CH_4/O_2 on 2.5 wt% Ir/Al_2O_3 (on-line MS analysis is shown in figure 4(a)).

3.3. Comparison of the structural changes of Ir/Al_2O_3 catalysts after treatments in steps I, II, and III

The different behavior of the two catalysts also becomes evident from the room temperature EXAFS data shown in figure 7. The whiteline of the 0.5 wt% Ir/Al_2O_3 catalyst after treatment in the CH_4/O_2 reaction mixture (full line in figure 7 (b) and (d)) is much higher compared to that of the same catalyst after reduction in H_2/N_2 (dashed lines in figure 7 (b) and (d)). In contrast, for the 2.5 wt% Ir/Al_2O_3 catalyst the difference of the catalyst after H_2/N_2 (dashed lines in figure 7 (a) and (c)) and CH_4/O_2 (solid line in figure 7 (a) and (c)) treatments is small. When heating the catalysts a second time in the CH_4/O_2 reaction mixture to 600 °C, a reversible behavior was found. No structural differences and no shift of the ignition temperature was observed when varying the flow (the residence time). Also in the case of the Rh/Al_2O_3 catalyst [26], we did not find changes and it seems that the particle structure is very similar at different residence times. However, the selectivity towards CO/H_2 is normally improved when using shorter residence times.

The structural changes during step I to III are schematically summarized in figure 8 (a) and (b). The decomposition upon He and H_2/N_2 treatment is quite similar in both cases, but it has been shown in section 3.1 that metallic Ir particles form already during He treatment in the case of high Ir loadings, while in the case of low loadings most of the Ir clusters are reduced during the reduction step in H_2/N_2. It was also shown that the dispersion of the metallic Ir clusters is higher at lower loading (*cf.* tables 1 and 2).

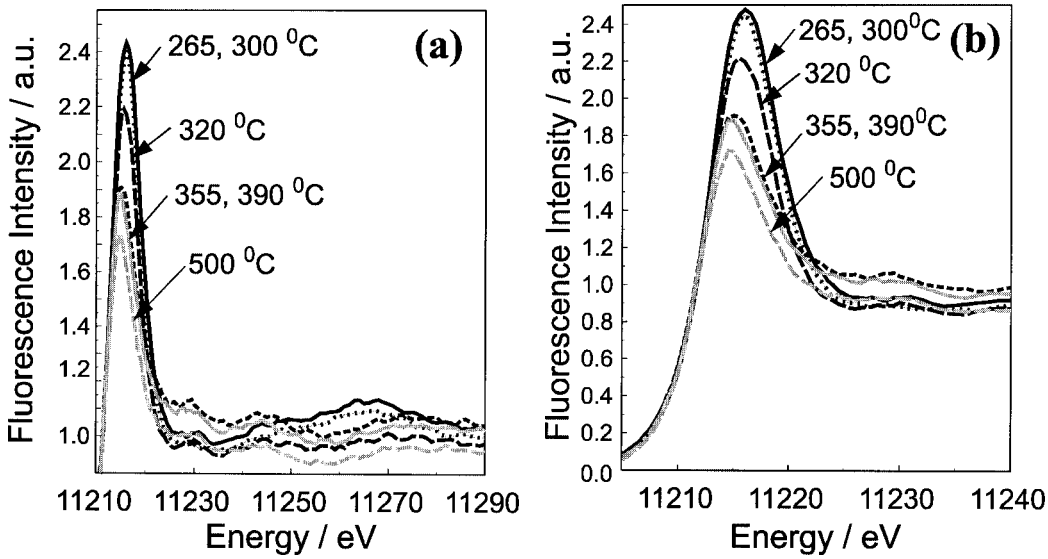

Figure 6. Selected *in situ* XANES data (fluorescence detection) at the Ir L_3 edge below and above the ignition temperature of the CPO reaction in the reaction mixture CH_4/O_2 on 0.5 wt% Ir/Al_2O_3 (on-line MS analysis is shown in figure 4(b)).

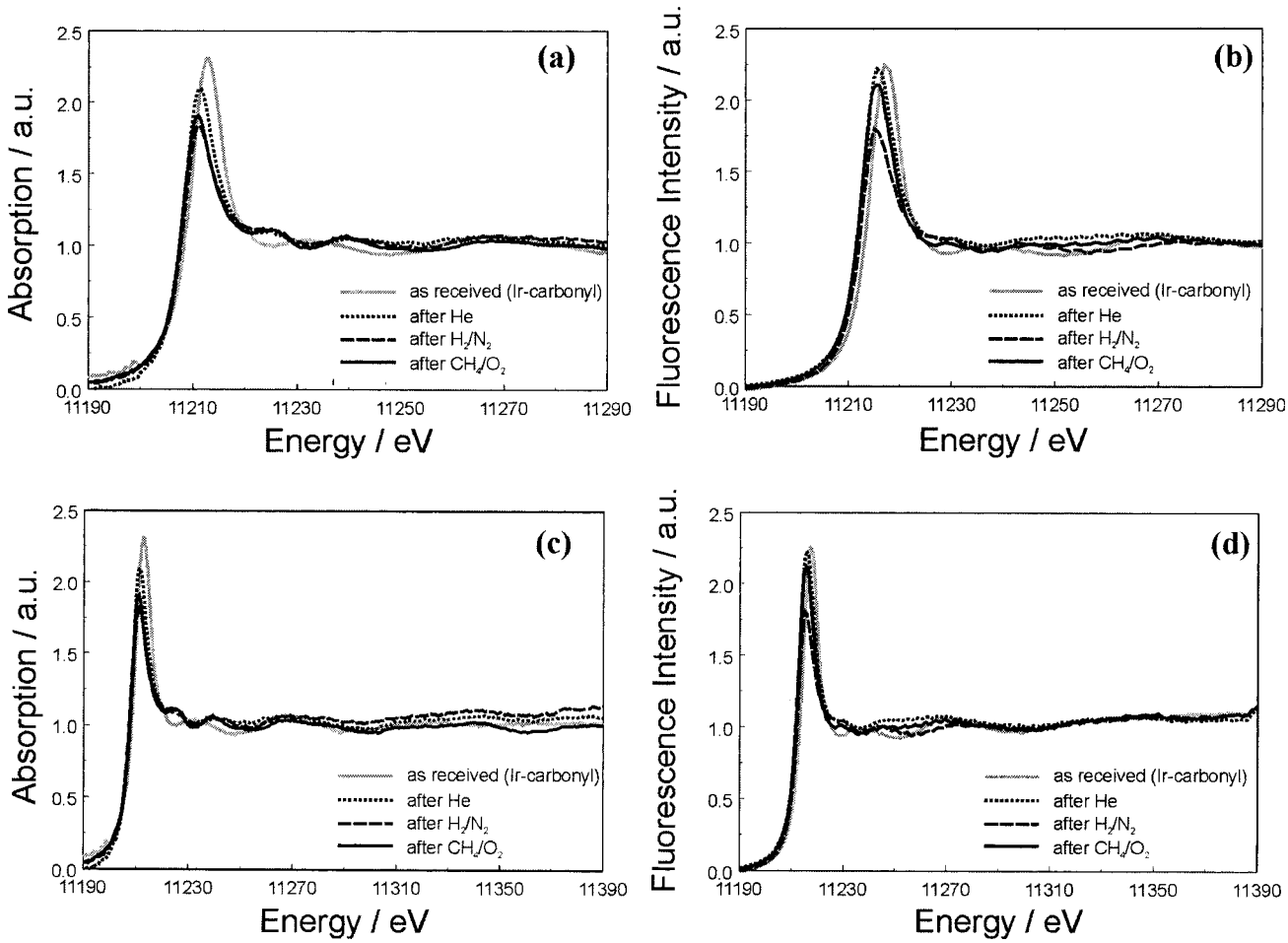

Figure 7. *In situ* EXAFS spectra at room temperature of the catalyst samples as received (gray solid line), after step I (He, dotted line), after step II (H_2, dashed line) and after step III (CH_4/O_2, solid line) on (a, c) 2.5 wt% Ir/Al_2O_3 in the transmission mode, and (b, d) 0.5 wt% Ir/Al_2O_3 with fluorescence detection.

The structural changes in steps I and II are supported by DRIFTS studies performed on low loaded Ir catalysts, as discussed in section 3.1. When heating in the CH_4/O_2 reaction mixture reversible structural changes occur: (a) oxidation of the Ir clusters below the ignition temperature and (b) reduction above the ignition temperature, as indicated in figure 8. DRIFTS studies revealed some carbonyl species being formed on the surface for Ir/Al_2O_3 samples above the ignition temperature [7].

The reversible structural changes during heating in the reaction mixture and the abrupt reduction of the clusters at the ignition temperature are similar to those on Rh/Al_2O_3 catalysts identified by XAFS and DRIFTS [4,26]. Also in case of Rh clusters on alumina, some oxidation of Rh in the reaction mixture below the ignition point was observed. Similar to sample A, the Rh clusters were stable against oxidation during quenching in the reaction mixture to room temperature. In both cases the loading is high (2.5 wt% Ir/Al_2O_3, and 5 wt% Rh/Al_2O_3) and XAFS clearly shows that the noble metals Ir and Rh, respectively, are in the metallic state after quenching to room temperature (*cf.* figure 7 (a) and (c)). They oxidize only partly when heated in the reaction mixture up to 320 °C. A different behavior is observed on 0.5 wt% Ir/Al_2O_3. Even when the catalyst is rapidly cooled to room temperature, the Ir particles oxidize significantly, probably due to oxygen present in the feed gas and due to higher reactivity of the clusters. This enhanced sensitivity towards oxygen is most likely due to a smaller particle size of the metal clusters, as also supported by the coordination number (table 2). Also the comparison of 5 wt% Rh/Al_2O_3 studied by XAFS [26] and 0.1 wt% Rh/Al_2O_3 studied by DRIFTS [7] has indicated that the reactivity of the clusters increases with a low loading. Although the particle size at room temperature is smaller for the low loading Ir catalysts, during heating to higher temperatures in the reaction atmosphere, redispersion effects may occur in case of higher loading Ir catalysts, as we have shown in a previous study for Rh/Al_2O_3 catalysts [7,26].

The *in situ* fluorescence XAFS results on noble metal based catalysts, combined with on-line catalytic measurements and supported by DRIFTS and transmission XAFS experiments, show not only the importance of studying the structural changes under reaction conditions. These studies also give the opportunity to consider the influence of the noble metal loading, which probably has a strong effect on the dispersion and, therefore, the reactivity of the clusters.

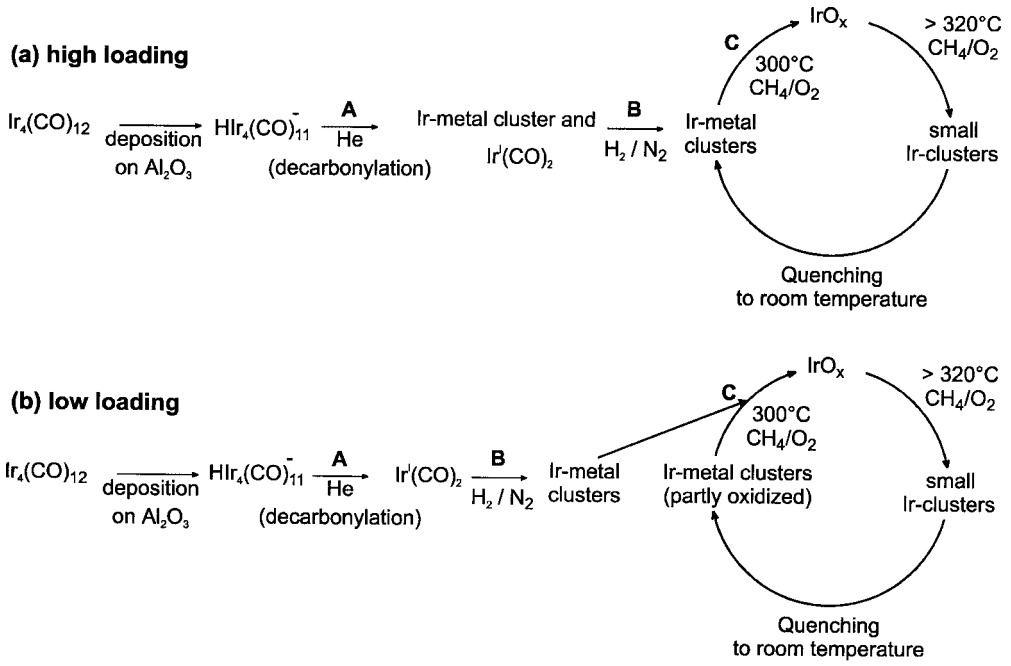

Figure 8. Schematic representations of the structural changes during steps I–III for catalyst samples with (a) high Ir-carbonyl loading (*i.e.*, sample A) and (b) low Ir-carbonyl loading Ir concentrations (*i.e.*, sample B); for more details, see text.

4. Conclusions

The novel setup for X-ray absorption fine structure combined with on-line mass spectrometry has given *simultaneous* insight into the structural properties (particle size, oxidation state) and the catalysis of small Ir clusters. The capillary setup is ideal for such studies and can be applied both during *in situ* fluorescence and transmission XAFS experiments. Fluorescence XAFS showed that the investigation of catalysts with an Ir loading of 0.5 wt% Ir can be well performed. Not only the XANES region, which gave information on the oxidation state of the Ir catalysts during time resolved studies, but also the EXAFS oscillations were resolved, so that additional information on the Ir cluster structure could be extracted. The silicon drift detector for the acquisition of the fluorescence X-rays is useful for these studies since it is less bulky than many other fluorescence detectors and can handle high count rates with the *in situ* cell setup. This detector may be interesting for further studies on promoters, poisons, and noble metals being present in very small concentrations on the catalysts. Currently, a 61-element module is under development, which will be even more interesting for these studies.

The results have revealed interesting differences in the structure and reactivity of Ir clusters when different loadings were used and they supplement conclusions obtained by transmission EXAFS and DRIFTS on Rh/Al_2O_3 catalysts. The structural changes are summarized in scheme 8 (a) and (b). $Ir_4(CO)_{12}$ deposited on alumina and forming $HIr_4(CO)_{11}^-$ decomposed only to metallic Ir clusters under He treatment, when the Ir loading was high. In the case of low loadings, probably carbonylic/oxidic species, such as $Ir^I(CO)_2$, form on the surface, which is further decomposed to Ir metal during TPR in hydrogen. In catalysts containing 0.5 wt% Ir, the Ir clusters are more easily oxidized than at higher loadings, where only partly oxidation in the reaction mixture below the ignition temperature is observed. Above the ignition temperature of the CPO reaction the clusters are reduced to metallic clusters in both cases. Similar to Rh/Al_2O_3 catalysts, the structural changes are reversible.

Acknowledgment

The authors thank HASYLAB for offering beamtime at beamline X1. We are grateful to L. Tröger with regard to fluorescence EXAFS measurements, A. Kjersgaard and S. Rokni for their help throughout the XAFS experiments and K. Aasberg-Petersen for helpful discussions. Financial support from DANSYNC (JDG, BSC) is gratefully acknowledged.

References

[1] G.A. Foulds and J.A. Lapszewicz, in: *Catalysis*, Vol. 11 (The Royal Society of Chemistry, Cambridge, 1994) p. 412.
[2] A.T. Ashcroft, A.K. Cheetham, M.L.H. Green and P.D.F. Vernon, Nature 352 (1991).
[3] J.A. Lapszewicz and X.-Z. Jiang, Prepr. Am. Chem. Soc. Div. Pet. Chem. 38 (1993) 815.
[4] L. Basini and A. Aragno, J. Chem. Soc. Faraday Trans. 90 (1994) 787.
[5] D.A. Hickman and L.D. Schmidt, J. Catal. 138 (1992) 267.
[6] D.A. Hickman and L.D. Schmidt, Science 259 (1993) 343.
[7] L. Basini, A. Aragno and G. Vlaic, Catal. Lett. 39 (1996) 49.
[8] L. Basini, A. Guarinoni and A. Aragno, J. Catal. 190 (2000) 284.
[9] L. Basini, M. Marchionna and A. Aragno, J. Phys. Chem. 96 (1992) 9431.
[10] S.D. Maloney, F.B.M.V. Zon, M.J. Kelley, D.C. Koningsberger and B.C. Gates, Catal. Lett. 5 (1990) 161.

[11] S.D. Maloney, M.J. Kelley, D.C. Koningsberger and B.C. Gates, J. Phys. Chem. 95 (1991) 9406.
[12] L. Basini and D. Sanfilippo, J. Catal. 157 (1995) 162.
[13] S. Kawi, J.-R. Chang and B.C. Gates, J. Phys. Chem. 97 (1993) 5375.
[14] A. Zhao and B.C. Gates, J. Catal. 168 (1997) 60.
[15] W.A. Weber, A. Zhao and B.C. Gates, J. Catal. 182 (1999) 13.
[16] L. Basini, A. Guarinoni and K. Aasberg-Petersen, Stud. Surf. Sci. Catal. 119 (1998) 699.
[17] R. Prins and D.C. Koningsberger, in: *X-ray Absorption: Principles, Applications, Techniques of EXAFS, SEXAFS and XANES*, eds. D.C. Koningsberger and R. Prins (Wiley, New York, 1988) p. 321.
[18] Y. Iwasawa, *X-ray Absorption Fine Structure for Catalysts and Surfaces*, Vol. 2 (World Scientific, Singapore, 1996).
[19] B.S. Clausen, H. Topsøe and R. Frahm, Adv. Catal. 42 (1998) 315.
[20] B.S. Clausen and H. Topsøe, Catal. Today 9 (1991) 189.
[21] J.W. Couves, J.M. Thomas, D. Waller, R.H. Jones, A.J. Dent, G.E. Derbyshire and G.N. Greaves, Nature 354 (1991) 465.
[22] J.-D. Grunwaldt, A.M. Molenbroek, N.-Y. Topsøe, H. Topsøe and B.S. Clausen, J. Catal. 194 (2000) 452.
[23] J.M. Thomas and G. Sankar, J. Synchr. Rad. 8 (2001) 55.
[24] J.-D. Grunwaldt and B.S. Clausen, Topics Catal. (2001), in press.
[25] K.K. Bando, T. Saito, K. Sato, T. Tanaka, F. Dumeignil, M. Imanura, N. Matsubayashi and H. Shimada, J. Synchr. Rad. 8 (2001) 581.
[26] J.-D. Grunwaldt, L. Basini and B.S. Clausen, J. Catal. (2001), in press.
[27] J. Jaklevic, J.A. Kirby, M.P. Klein, A.S. Robertson, G.S. Brown and P. Eisenberger, Solid State Commun. 23 (1977) 679.
[28] F.W. Lytle, R.B. Greegor, D.R. Sandstrom, E.C. Marques, J. Wong, C.L. Spiro, G.P. Huffman and F.E. Huggins, Nucl. Instrum. Methods Phys. Res. 226 (1984) 542.
[29] P. Kappen, J.-D. Grunwaldt, B.S. Hammershøj, L. Tröger, G. Materlik and B.S. Clausen, J. Catal. 198 (2001) 56.
[30] P. Kappen, L. Tröger, H. Zink, G. Materlik, C. Reckleben, K. Hansen, J.-D. Grunwaldt and B.S. Clausen, HASYLAB Annual Report 1999 (2000).
[31] J.-D. Grunwaldt, P. Kappen, B.S. Hammershøj, L. Tröger and B.S. Clausen, J. Synchr. Rad. 8 (2001) 572.
[32] B.S. Clausen, G. Steffensen, B. Fabius, J. Villadsen, R. Feidenhans'l and H. Topsøe, J. Catal. 132 (1991) 524.
[33] B.S. Clausen, L. Gråbæk, G. Steffensen, P.L. Hansen and H. Topsøe, Catal. Lett. 20 (1993) 23.
[34] B. Lengeler, J. Phys. (Paris) C8 (1986) 75.
[35] F.B. Duivenvoorden, D.C. Koningsberger, Y.S. Uh and B.C. Gates, J. Am. Chem. Soc. 108 (1996) 6254.
[36] K. Tanaka, K.L. Watters and R.F. Howe, J. Catal. 75 (1982) 23.
[37] M. Alibrando, H.S. Hahm and E.E. Wolf, Catal. Lett. 49 (1997) 1.